

Supporting Information

Biomass based flexible nanoscale carbon fibers: effects of chemical structure on energy storage properties

Hao Zheng, Qiping Cao, Mengni Zhu, Dang Xu, Haoyu Guo, Yao Li*, Jinghui Zhou*

Liaoning Province Key Laboratory of Pulp and Papermaking Engineering, Dalian Polytechnic University, Dalian, Liaoning Province, 116034, P. R. China.

* To whom correspondence should be addressed.

China. E-mail: liyaodlpu@163.com

China. E-mail: zhoujh@dlpu.edu.cn

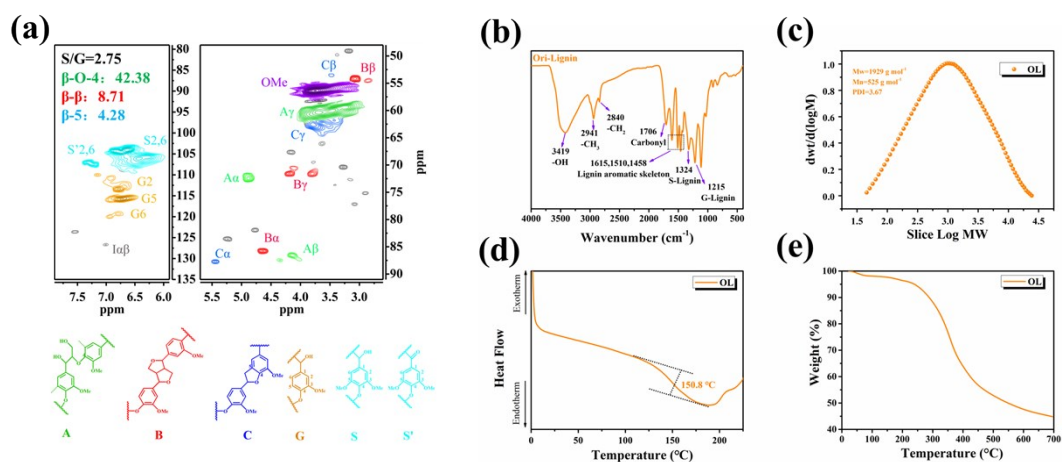


Fig. S1 Basic properties of original lignin (a) 2D-HSQC NMR spectra, (b) FT-IR spectra, (c) GPC chromatograms, and (d) DSC spectra and (e) TGA spectra

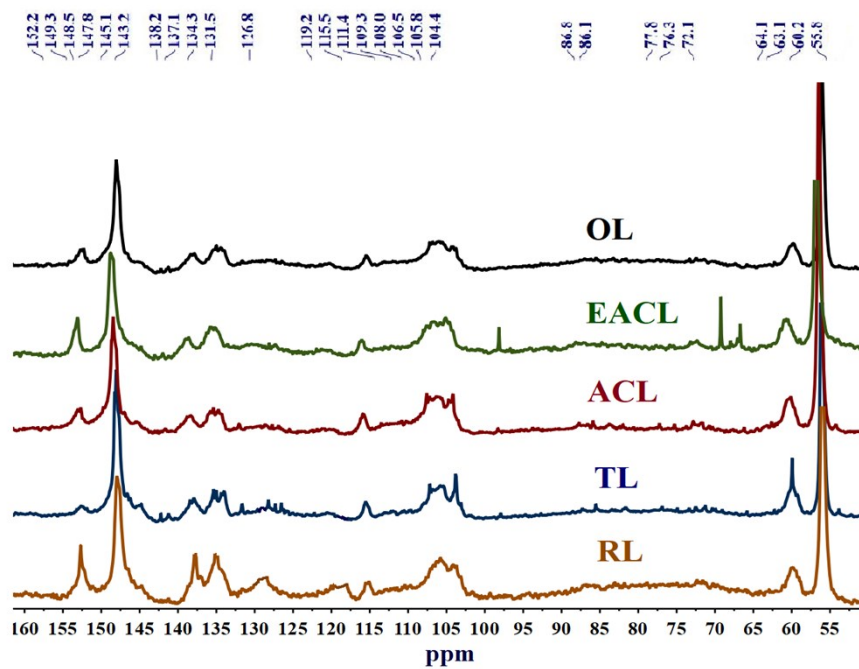


Fig. S2 Quantitative ^{13}C NMR spectra of the OL, EAACL, ACL, TL and RL

Table S1 Assignment and quantification of the signals of the ^{13}C -NMR spectra (results expressed per Ar)

δ	Assignment	OL	EACL	ACL	TL	RL
155.0–140.0	Aromatic C–O	2.34	3.11	2.79	2.81	1.16
140.0–124.0	Aromatic C–C	1.32	1.16	0.94	1.71	4.37
124.0–102.0	Aromatic C–H	2.32	2.89	1.47	1.53	2.29
61.3–58.0	β -O-4' linkages	0.43	0.36	0.84	0.98	0.77
58.0–54.0	CH_3O	5.46	4.28	3.53	3.21	3.03

The hydroxyl groups in lignin are quantitatively characterized by ^{31}P -NMR. The sample preparation steps are as follows: firstly, prepare the mixed solution of deuterated pyridine/deuterated chloroform (1.6:1, V/V), weigh 40mg of deuterated alcohol, use the above mixed solution of deuterated pyridine/deuterated chloroform to 1mL, and fully dissolve as the internal standard solution. 40 mg lignin sample is weighed and dissolved in 800 μL deuterated pyridine/deuterated chloroform mixed solution, 100 μL internal standard solution and 130 μL phosphitylating reagent (2-chloro-4,4,5,5-tetramethyl-1,3,2-dioxaphospholane TMDP) are added sequentially. After reaction for 2 h, the lignin sample is fully phosphated and detected by nuclear magnetic resonance spectroscopy. Mestrenova software is used to process the data of the spectrogram, and the peak position is corrected by determining the position of the alcohol peak at (δ P145). The quantitative value of the hydroxyl group per unit mass of lignin is obtained by multiplying the integral value by 0.2586 (molecular weight of silyl alcohol is 386.65 g/mol). All chemical shifts reported are relative to the reaction

product of water with tetramethyldioxaphospholane, which has been observed to give a sharp signal in pyridine/ CDCl_3 at 132.2 ppm. More details regarding quantitatively characterized of the hydroxyl groups in lignin chemicals analysis are given in the Supporting Information (**Fig. S3 and Table S2**).

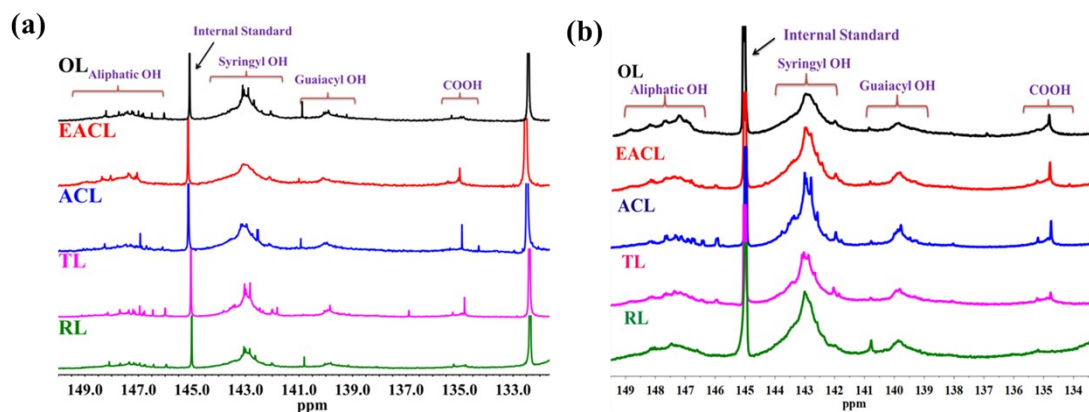


Fig. S3 ^{31}P -NMR spectra of TMDP (a) and H_3PO_4 (b) phosphitylated OL, EACL, ACL, TL

Table S2 Functional groups of lignins as determined by quantitative ^{31}P -NMR (mmol/g)

Samples	OL	EACL	ACL	TL	RL
Aliphatic OH	1.09	1.22	0.92	0.83	1.06
Syringyl OH	2.29	0.85	1.86	2.47	1.27
Guaiacyl OH	0.85	0.27	0.68	0.87	0.33
Total phenolic OH	3.14	1.12	2.54	3.34	1.60
COOH	0.12	0.13	0.11	0.06	0.09

To further characterize the effect of H_3PO_4 on the content of lignin hydroxyl, the functional groups of the phosphide lignin fractions are calculated according to the ^{31}P -NMR spectra in **Fig. S3b** and the results are listed in **Table S3**.¹ The ^{31}P -NMR chemical shifts range of these phosphitylated alcohols is located at 145.2–147.1 ppm which overlapped with the aliphatic OHs in lignin (usually from 145.4 to 150.0 ppm). In this study, the content of phenolic hydroxyl groups in OL, EACL, ACL, TL and RL after phosphating is determined to be 1.07, 1.47, 1.03, 0.71 and 0.89 mmol/g, respectively. In comparison with the unphosphating lignin shows lower content of phenolic hydroxyl groups, which are estimated to be 2.29, 0.85, 1.86, 2.47 and 1.27 mmol/g. However, the content of alcohol hydroxyl changes little, which indicates that phosphating reaction mainly affects phenolic hydroxyl group of lignin. Poplar lignin powders are separated and purified by different organic solvents. Compared with other lignin samples, the phenolic hydroxyl content (0.71 mmol/g) of tetrahydrofuran phase lignin (TL) is decreased by 0.36 mmol/g compared with original lignin (OL,

1.07 mmol/g). The decrease of phenolic hydroxyl content indicates that TL lignin has the strongest interaction with phosphoric acid. This combination not only improves the spinning properties of poplar lignin, but also shows excellent thermal stability during heat treatment.

Table S3 Functional groups of phosphatizing lignin samples as determined by quantitative ^{31}P -NMR (mmol/g)

Samples	OL	EACL	ACL	TL	RL
Aliphatic OH	0.45	0.47	0.46	0.43	0.41
Syringyl OH	1.07	1.47	1.03	0.71	0.89
Guaiacyl OH	0.34	0.43	0.34	0.22	0.46
Total phenolic OH	1.41	1.90	1.37	0.93	1.35
COOH	0.14	0.21	0.21	0.11	0.19

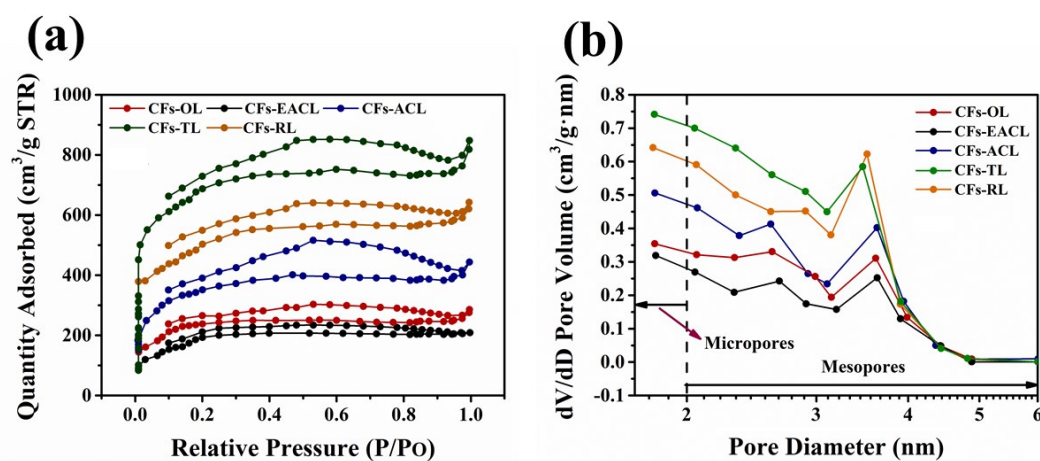


Fig. S4 (a) Nitrogen adsorption-desorption isotherms and (b) pore size distribution of the biomass-based CFs prepared with different fraction samples

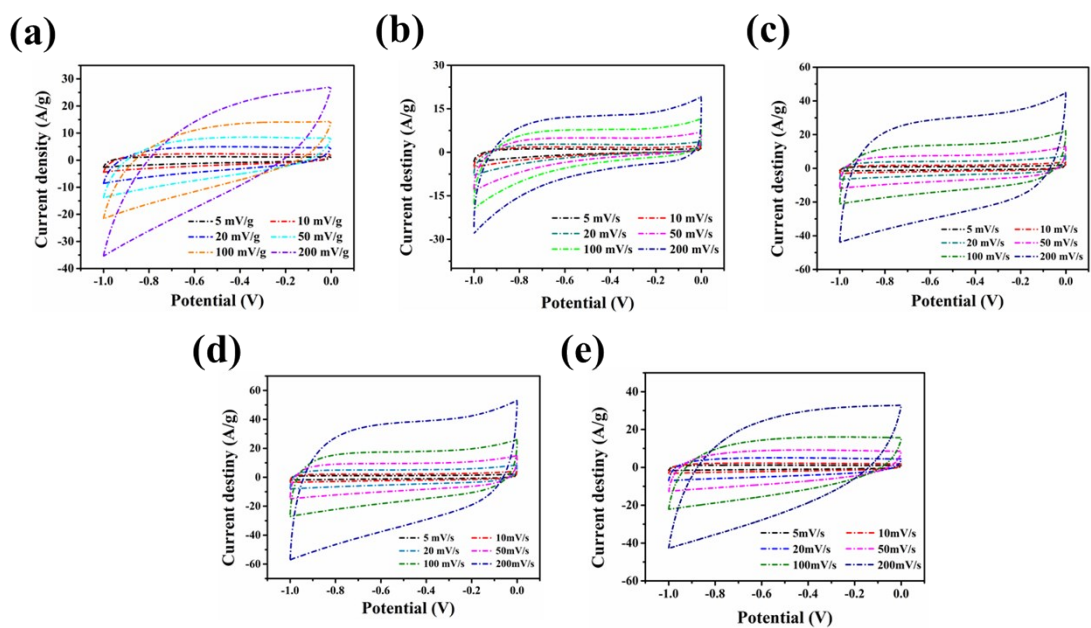


Fig. S5 CV curves of (a) CFs-OL, (b) CFs-EACL (c) CFs-ACL, (d) CFs-TL, and (e) CFs-RL at a scan rate of 5, 10, 20, 50, 100 and 200 mV/s, respectively

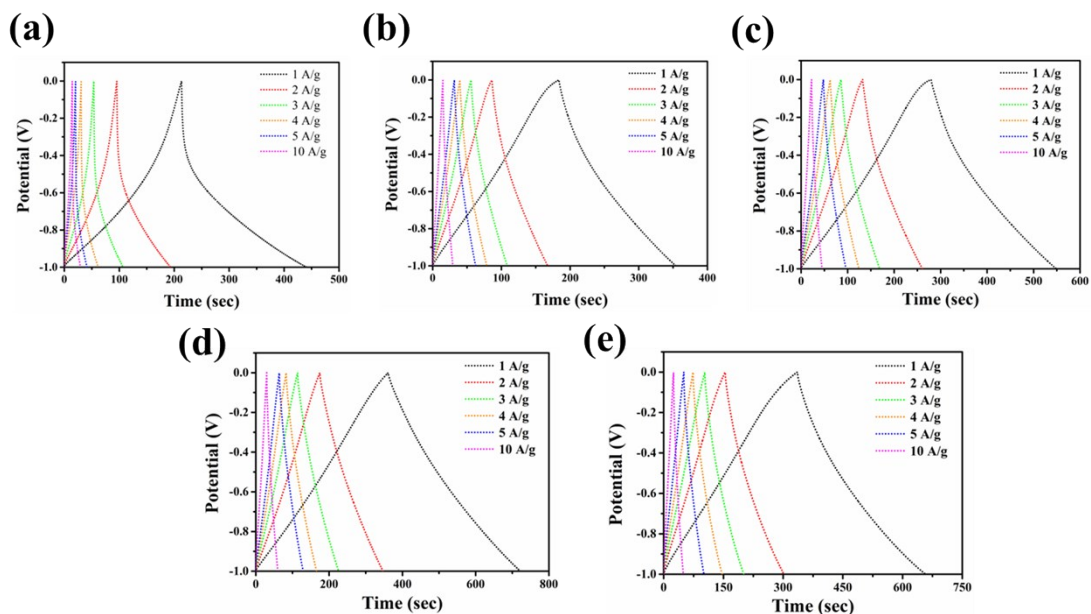


Fig. S6 GCD curves of (a) CFs-OL, (b) CFs-EACL (c) CFs-ACL, (d) CFs-TL, and (e) CFs-RL at current density of 1, 2, 3, 4, 5 and 10 A/g, respectively

The calculation of Faradaic process at different scan rates using the following equation:²

$$a) i = av^{1/2} + bv \quad S1$$

$$b) i/v^{1/2} = a + b v^{1/2} \quad S2$$

Where v is scan rate (mV/s), a and b are constants. $av^{1/2}$ and bv are belongs to current contribution of capacitive charge storage and diffusion-control Faradaic process, respectively.

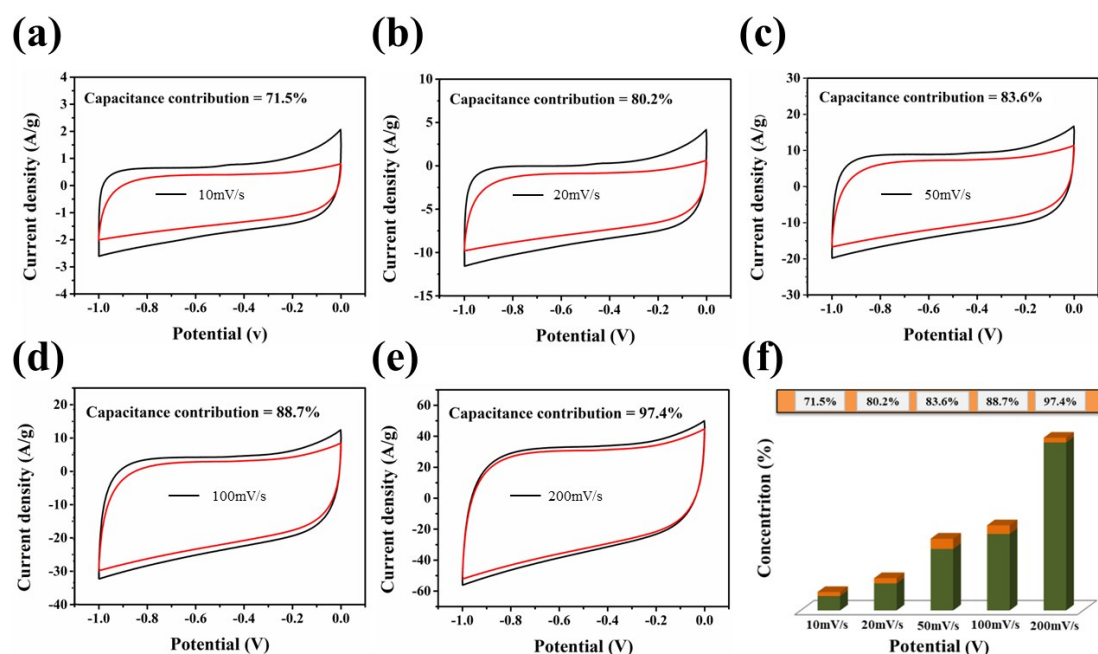


Fig. S7 (a~e) Capacitive contribution (red region) of the CFs-TL to the total current at the current density of 10, 20, 50, 100, and 200 mV/s; (f) Contribution ratio of capacitive charge storage and diffusion-control Faradaic process of CFs-TL electrode at different scan rates

In order to further investigate the application potential in the field of energy storage, the biomass-based CFs is directly used as free-standing archetype electrodes (size about 1.0 cm²). The electrochemical capacitive performance of three-electrode is

evaluated by cyclic voltammetry (CV) and galvanostatic charge/discharge (GCD) measurement. **Fig. S8** shows the CV curves with the biomass-based CFs as free-standing electrode directly at scan rates of 5, 10, 20, 50, 100 and 200 mV/s. At the high scan rates of 200 mV/s, the CV profiles of the CFs-TL maintain the rectangular shape of the voltammograms with little distortion, which can be attributed to the excellent electrical conductivity and the low mass transport resistance. On the contrary, the CV curves of other samples at varied potential scan rates exhibit a slight polarization phenomenon and a much smaller area. These results are attributed to the low conductivity and hydrophobicity of the carbon-based materials.

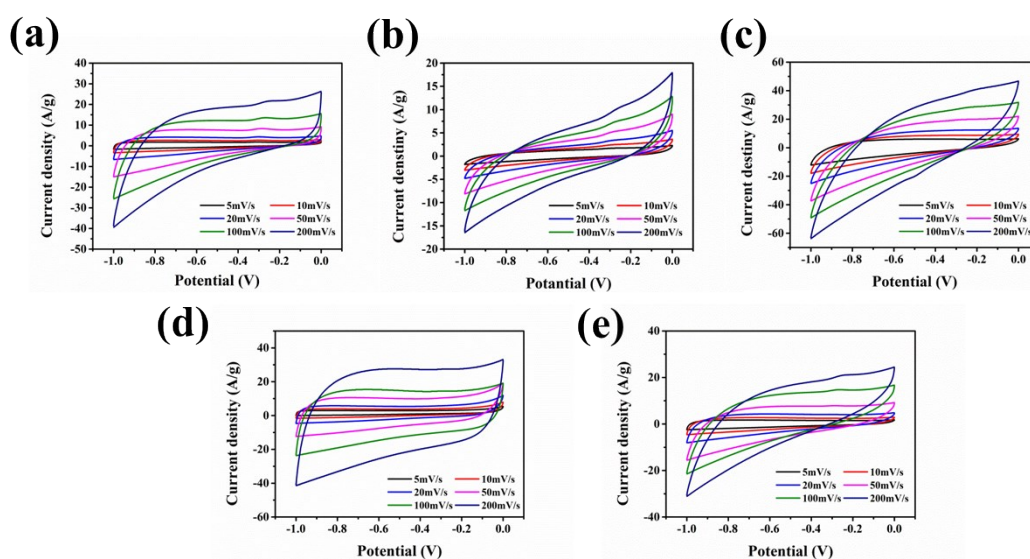


Fig. S8 CV curves of (a) CFs-OL, (b) CFs-EACL (c) CFs-ACL, (d) CFs-TL, and (e) CFs-RL as free-standing electrodes at a scan rate of 5, 10, 20, 50, 100 and 200 mV/s, respectively

Fig S9 shows the GCD curves at different current densities (1~5 A/g). Rate capability of CFs-OL, CFs-EACL, CFs-ACL, CFs-TL and CFs-RL as free-standing electrode directly are depicted. The capacitance retention of CFs-TL is 78.2% with the current density to 5 A/g, while the capacitance retention of CFs-OL under the same

current density is only 43.3%. The enhancement of the rate capability for the CFs-TL is mainly attributed to the improved conductivity which facilitating the electron transportation, resulting in a faster electronic response.

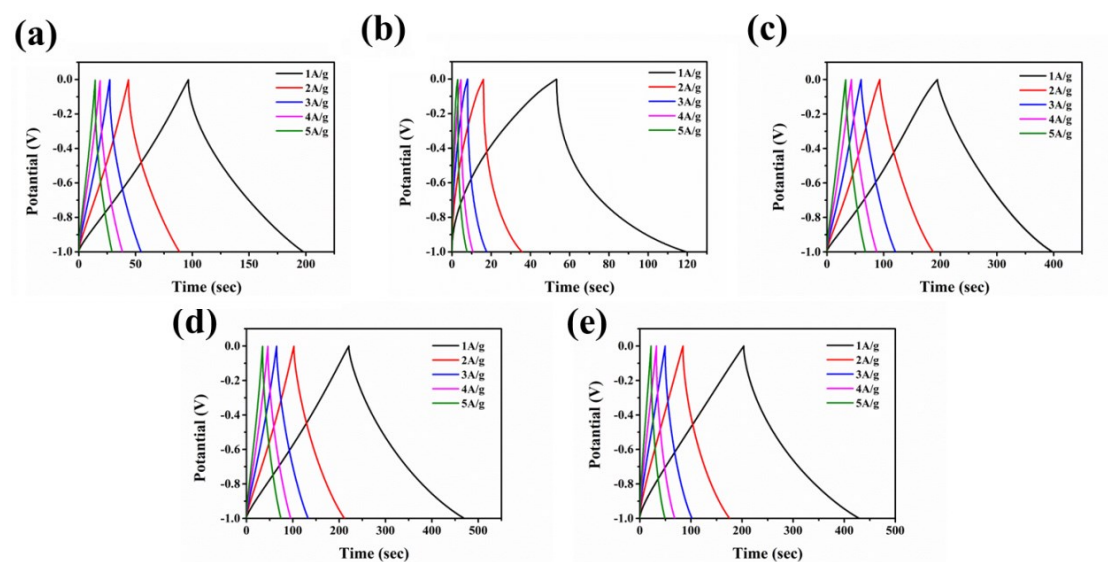


Fig. S9 GCD curves of (a) CFs-OL, (b) CFs-EACL (c) CFs-ACL, (d) CFs-TL, and (e) CFs-RL as free-standing electrodes at current density of 1, 2, 3, 4 and 5 A/g, respectively

To investigate the cycling stability, CV and GCD tests are performed at a current density of 1 A/g (**Fig. S10a and 10b**). The specific capacitance of the CFs-OL, CFs-EACL, CFs-ACL CFs-TL, and CFs-RL as three-electrode capacitance reaches 135.5, 89.6, 168.2, 252, and 219 F/g, respectively. The CFs-TL exhibits a larger of enclosed area and long discharging time than other biomass-based CFs (**Fig. S10c**). Cycle stability demonstrates that the specific capacitance of CFs-TL retains about 98% after 10000 charging/discharging cycles (**Fig. S10d**). To gain more insight, the batteries are studied by electrochemical impedance spectroscopy (EIS), and the collected Nyquist plots are displayed in **Fig 10e**. The semicircles in the high frequency region represent

the charge transfer impedance (Rct), which indicates the difficulty of charge transfer at the interface between the electrodes and electrolyte. Clearly, the Rct has no obvious change with increasing cycle number, which is probably due to the stability of carbon fiber electrode material. These results reveal that this type of porous nanostructure and high graphitization degree could facilitate the electrolyte ion diffusion and electron transportation, leading to a reduced internal resistance and an improved electrochemical performance.

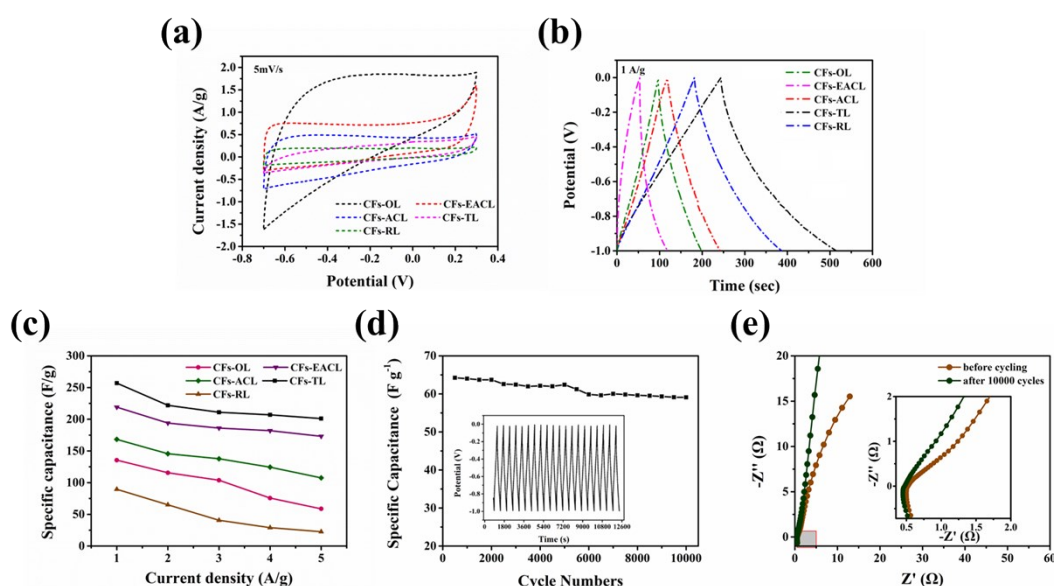


Fig. S10 (a) CV curves of the biomass-based CFs as free-standing electrodes at a scan rate of 5 mV/s, (b) GCD curves of the biomass-based CFs at current density of 1 A/g, (c) gravimetric capacitances of the biomass-based CFs at different current densities, (d) Cycle performance of CFs-TL at 1 A g⁻¹ over 10000 cycles and the last 20 charge/discharge curves (inset d), and (e) Nyquist plots of CFs-TL before cycling, and after 10000 cycles

In order to simulate the actual device behavior, the double-electrode CV and GCD test are performed on CFs-TL using the same test method (**Fig. S11**). In Fig S10a and S10c, a suddenly current increase in 1.2V can be ascribed to water decomposition. The excellent specific capacitance of the double electrode capacitance

prepared by CFs-TL reaches 63 F/g and the high capacitance retention reaches 78.2% at current densities of 1 A/g (Fig. S11e). Energy density and power density as two additional important parameters for the evaluation of the entire device are shown in Fig. S10f. The CFs-TL exhibits a high energy density (26.5 Wh/kg) at the power density of 800 W/kg. Even when the power density increased to 8 KW/kg, the energy density of the CFs-TL remains at 21.1 Wh/kg.

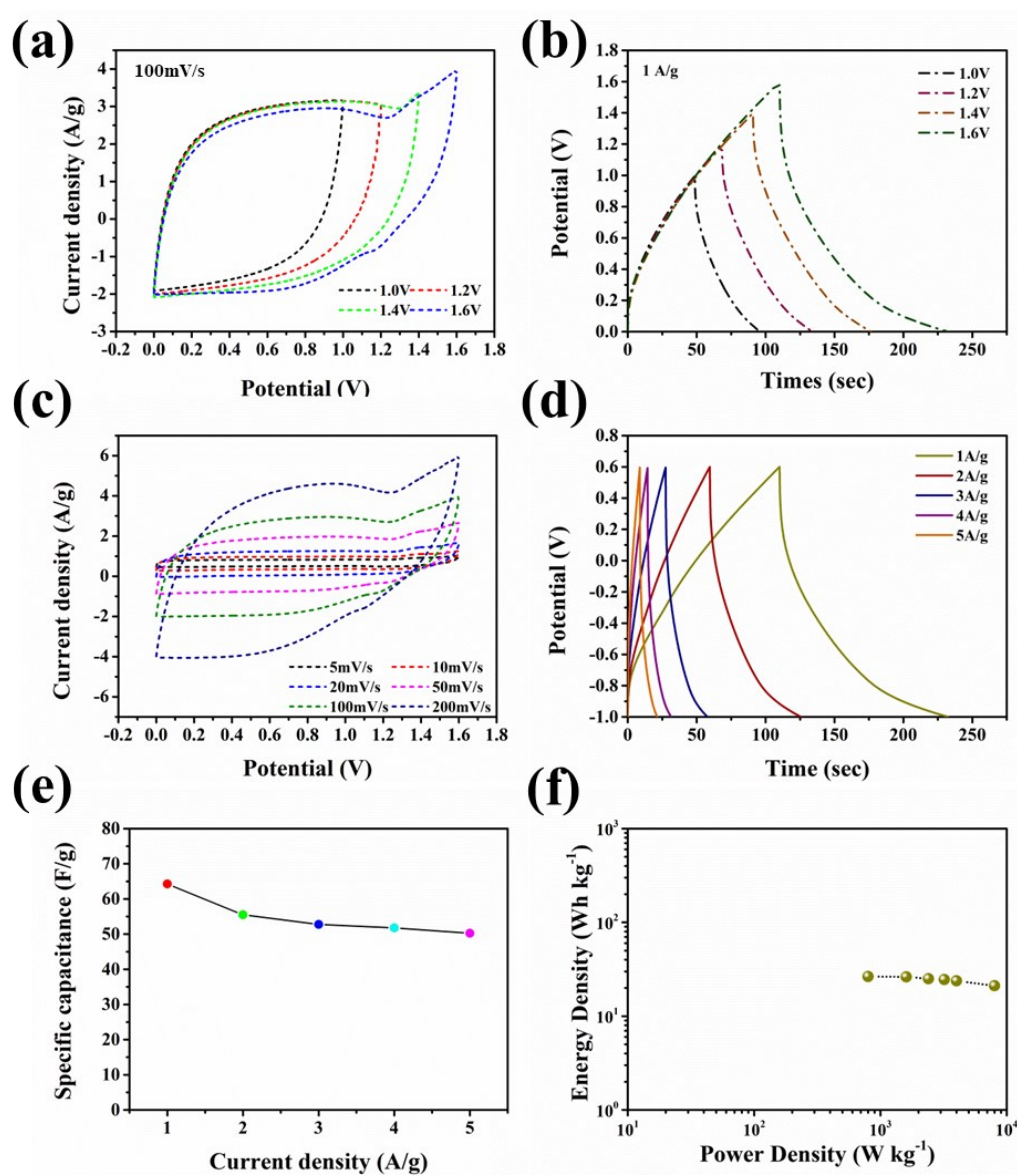


Fig. S11 Electrochemical properties of the CFs-TL as free-standing electrode measured in a double-electrode system using 1 mol/L Na₂SO₄. (a) CV curves at 100 mV/s and (b) GCD curves at

1 A/g of the electrode at different operation voltages, (c) CV curves at different scan rates from 5 to 200 mV/s, (d) GCD curves at different current densities from 1 to 5 A/g, (e) gravimetric capacitances at different current densities, (f) Ragone plots based on the supercapacitor of CFs-TL

References

- 1 Q. Cao, M. Zhu, J. Chen, Y. Song, Y. Li and J. Zhou, *ACS Appl. Mater. Interfaces*, 2019, **12**, 1210-1221.
- 2 M. Zhu, H. Liu, Q. Cao, H. Zheng, D. Xu, H. Guo, S. Wang, Y. Li and J. Zhou, *ACS Sustain. Chem. Eng*, 2020, **8**, 12831-12841.